THE JOURNAL OF PHYSICAL CHEMISTRY C

Article

Cite This: J. Phys. Chem. C 2018, 122, 6760−6773

pubs.acs.org/JPCC

# Modeling the Polymerization Process for Geopolymer Synthesis through Reactive Molecular Dynamics Simulations

Mo Zhang,[†,§] N. Aaron Deskins,*[,‡] Guoping Zhang,[∥] Randall T. Cygan,[⊥] and Mingjiang Tao*[,†]

[†]Department of Civil and Environmental Engineering and [‡]Department of Chemical Engineering, Worcester Polytechnic Institute, Worcester, Massachusetts 01609, United States

[§]Department of Civil and Safety Engineering, Dalian Jiaotong University, Dalian, Liaoning Province 116028, P. R. China

[∥]Department of Civil and Environmental Engineering, University of Massachusetts Amherst, 38 Marston Hall, 130 Natural Resources Road, Amherst, Massachusetts 01003-0724, United States

[⊥]Geochemistry and Materials Science Research, Sandia National Laboratories, Albuquerque, New Mexico 87185-0754, United States

**ABSTRACT:** Geopolymers are a class of inorganic aluminosilicate polymers composed of silicate and aluminate tetrahedrons that are linked by sharing oxygen atoms. A reactive molecular dynamics (MD) simulation approach was used to model the polymerization process and molecular structure of geopolymer gels. Reactive silicate and aluminate monomers were first optimized with density functional theory simulations and "polymerized" subsequently in MD models with a reactive Feuston and Garofalini potential. MD models with Si/Al molar ratios of 2 and 3 were simulated at temperatures ranging from 650 to 1800 K to investigate the effect of Si/Al ratio and temperature on the polymerization process and the properties of computationally synthesized "geopolymer gels". Geopolymer gels close to those produced experimentally were computationally "synthesized" for the first time. The distribution of $Si_4(mAl)$ and radial distribution functions of the modeled geopolymer gels showed good agreement with the respective experimental results of geopolymers in the literature. After a three-stage polymerization process, involving oligomerization, aggregation, and condensation, the molecular structure of geopolymer gels with the bulk density was obtained. A higher temperature enhanced the rate and degree of condensation and decreased the bulk density of final geopolymer gel structures, whereas a lower Si/Al ratio resulted in a more compact geopolymeric network.

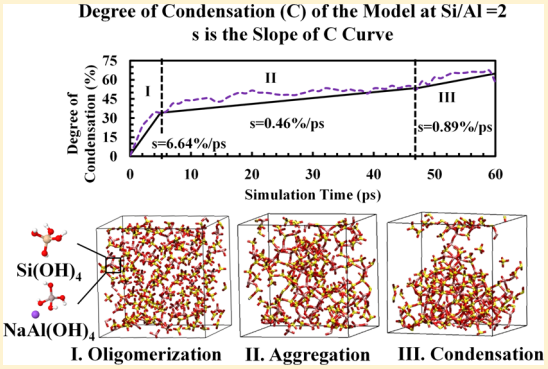


## 1. INTRODUCTION

Geopolymers or alkali-activated inorganic binders are a family of aluminosilicate materials with amorphous to semicrystalline molecular structures, which are composed of silicate and aluminate tetrahedrons that are cross-linked by shared oxygen atoms.[1] With high mechanical strength and up to 80% less $CO_2$ emission compared to ordinary Portland cement,[2,3] geopolymers have become a promising sustainable alternative to cement. Geopolymers can also be used in fire/acid-resistant coatings,[4−6] sewer pipes,[7] lightweight foam concrete,[8,9] toxic/radioactive contaminant encapsulation,[10] military operations,[11] railway sleepers,[12] and aircraft manufacturing[13] due to their excellent mechanical, physicochemical, and thermal properties. Geopolymers are usually synthesized using alkaline hydroxide and/or silicate solutions to activate aluminate- and silicate-rich materials, including natural minerals and industrial waste, such as metakaolin, fly ash, and blast furnace slag.[10,14−25]

The final product in the geopolymer synthesis is a composite material composed of unreacted raw materials, geopolymer gels, and zeolitic phases.[26,27] Among the above constituents, geopolymer gels are the most important because they act as a binding agent and largely govern mechanical properties of the resulting geopolymers. A simplified chemical formula $M_n\{-(SiO_2)_z-AlO_2-\}_n$ is used for approximately representing the molecular structures of geopolymers without knowing the molecular details, where M is the cation to balance the negatively charged $(Al(OH)_4)^{-1}$, such as sodium ($Na^+$) or potassium ($K^+$), and the subscript $z$ defines the Si-to-Al molar ratio, which is a vital factor in determining the mechanical properties of the resulting geopolymers. A variety of techniques have been employed to characterize geopolymer gels. For example, X-ray diffraction, scanning electron microscopy, and energy-dispersive X-ray spectroscopy have been used to qualitatively identify the formation of geopolymer gels.[1,28−30] However, none of these techniques can quantitatively define the geopolymers' chemical or molecular structures. Fourier transform infrared spectroscopy (FTIR) has been used to identify the formation of main chemical bonds, such as Si−O−T (T: Si or Al), Si−OH, and Al−OH, in geopolymer precursors, but the network and interconnectivity of these bonds are still a "puzzle".[31,32] Other methods such as nuclear magnetic resonance (NMR) spectroscopy can be used to assess

**Received:** January 24, 2018
**Revised:** March 2, 2018
**Published:** March 5, 2018





DOI: 10.1021/acs.jpcc.8b00697
J. Phys. Chem. C 2018, 122, 6760−6773

the coordination of Si and Al sites and investigate the change in chemical structures during geopolymerization, but some of the sites are difficult to distinguish.[33−35] X-ray/neutron pair distribution function (PDF) analysis has recently been used as a complementary tool to FTIR and NMR spectroscopies for examining the molecular structure of geopolymers.[36,37] Despite all of these efforts, a conclusive molecular structure of geopolymer gels remains elusive largely due to their amorphous nature.

The geopolymerization process is often approximated by the following highly simplified conceptual reactions:[1] (i) the raw materials are dissolved in alkali solutions, such as NaOH and KOH, to release the reactive aluminate and silicate monomers and (ii) the aluminosilicate oligomers polymerize in the alkali environment to form geopolymer gels. Because of the charge deficiency in Al (which has a $3^+$ charge compared to Si having $4^+$), cations of Na or K are needed to balance the presence of Al. Water is consumed during the dissolution of raw materials and released in the polymerization processes, which are schematically represented by eqs 1 and 2, respectively.

$$n(Si_2O_5,\ Al_2O_2) + 2nSiO_2 + 4nH_2O \xrightarrow{NaOH,KOH} n((OH)_3{-}Si{-}O{-}Al^{(-)}(OH)_2{-}O{-}Si{-}(OH)_3) \quad (1)$$

$$n((OH)_3{-}Si{-}O{-}Al^{(-)}(OH)_2{-}O{-}Si{-}(OH)_3) \xrightarrow{NaOH,KOH} (Na,\ K)_n^{(+)}{-}(Si(O^-){-}O{-}Al^{(-)}(O^-){-}O{-}Si(O^-){-}O{-})_n + 4nH_2O \quad (2)$$

It is hypothesized that the polymerization process (eq 2) includes a series of reactions that are intertwined with each other: (i) aluminate and silicate monomers are first polymerized to form oligomers with different sizes; (ii) large clusters and ring structures are subsequently formed by the gelation of the oligomers; and (iii) cross-linked structures are finally formed via the condensation of the clusters and rings.[27,38]

Zhang et al. investigated the geopolymerization processes by estimating the geopolymerization rate and degree using spectrometric analysis of the data obtained with an in situ energy-dispersive X-ray diffractometer and an isothermal conductive calorimeter.[40] Unfortunately, key aspects of the relationship between the molecular structure of geopolymer gels and the complex multistep geopolymerization process remain largely unknown. For instance, previous models of geopolymers relied on the thermodynamic parameters of zeolite analcime because the critical parameters of the geopolymeric structures were unavailable.[39,40] However, this relationship is of particular interest to tailor geopolymer synthesis for desired properties.

The amorphous nature of geopolymer gels presents technical challenges to molecular simulations, although molecular modeling in recent literature studies has provided some perspective to understand the geopolymeric structure and geopolymerization kinetics.[41] Zhang et al. used the semi-empirical AM1 method to study the dissolution, ion reorientation, and polycondensation processes of metakaolin-based geopolymers in a series of simulation studies.[42−44] Yang et al. used the density functional theory (DFT) method to assess the stability and structure of various aluminosilicate oligomers that are the basic units for geopolymerization. Subsequently, their group simulated the polymerization between a small oligomer (e.g., silicate monomer, aluminate monomer, or aluminosilicate dimer) and an aluminosilicate cluster (e.g., four, six, double four, or double six rings) to test the fundamental reaction mechanisms of geopolymerization.[45,46] These simulation studies have shed light on the initial pathways of how geopolymer structures were formed from raw materials, but were not able to obtain the final molecular structure of geopolymer gels comparable to those synthesized experimentally. This is because DFT modeling is limited to relatively small systems (e.g., those with perhaps hundreds of atoms), and realistically modeling geopolymer gels requires a much larger number of atoms. White et al. simulated aluminate and silicate oligomers with DFT simulations[47] and then applied their results in coarse-grained Monte Carlo (CGMC) simulations of alkali activation of metakaolin in three solutions with different silicate concentrations.[48] Their large-scale CGMC model was able to simulate the processes from the dissolution of raw materials to the initial polymerization of a Na-metakaolin-based geopolymer precursor system. Most of the aforementioned simulations focused on the early stage of the entire geopolymerization process, whereas geopolymer gels with molecular structures close to those synthesized in the laboratory have not been generated.[49]

Molecular dynamics (MD) modeling with a reactive potential by Feuston and Garofalini (FG potential)[50] was conducted to simulate the polymerization and condensation processes of silicate and aluminate monomers. Previously, the FG potential was used to model the polymerization of silicic acid ($Si(OH)_4$) and the effect of simulation temperature and silicic acid's concentration on the degree of polymerization.[51,52] Similar to the polymerization of silicic acid, the dimerization of silicate monomers and aluminate monomers is the essential reaction for the polymerization process in geopolymer synthesis.[47] Therefore, the FG potential was selected in the current work to investigate: (i) the molecular structure change of the aluminosilicate system during the polymerization; (ii) the molecular structure of computationally synthesized geopolymer gels; and (iii) the effect of chemical composition and simulation temperature on reaction kinetics and the molecular structures of the resulting geopolymer gels. It should be noted that there are some other reactive force fields, such as ReaxFF that has been widely used in silica polymerization. However, the FG potential is a simpler reactive force field and has been implemented in TREMOLO-X, so it was a logical choice for this work.

This article is organized as follows: the molecular model and simulation details are introduced in Section 2, including the potentials and theory used in this study; the simulation results are discussed and compared with experimental results in the literature in Section 3; and Section 4 presents the conclusions drawn from this study and suggestions for the future work.

## 2. METHODS

Molecular dynamics (MD) simulations were carried out to model the polymerization process from aluminate and silicate monomers ($NaAl(OH)_4$ and $Si(OH)_4$) to the resulting geopolymer gels. The dissolution of raw materials (e.g., metakaolin and fly ash) was omitted because it is practically impossible to simulate the entire geopolymerization process



DOI: 10.1021/acs.jpcc.8b00697
J. Phys. Chem. C 2018, 122, 6760−6773

with reactive MD modeling. Instead, silicate and aluminate monomers were optimized first with the density functional theory (DFT) method, as implemented in the CP2K package,[53,54] to represent the reactive components released from the dissolution stage. This approximation was based on the rationale that these monomers are energetically favorable as geopolymer precursors after the dissolution process. Subsequently, the optimized silicate and aluminate monomers were used as the building blocks to simulate the polymerization process using MD modeling with the FG potential. Simulation temperatures from 650 to 1800 K were applied to systems with Si/Al ratios of 2 and 3 to investigate the effect of temperature and chemical composition on the polymerization kinetics and molecular structures of computationally predicted geopolymer gels.

**2.1. Molecular Dynamics Simulations.** *2.1.1. Potentials.* The reactive Feuston−Garofalini (FG) interatomic potentials for Si, O, H, Na, and Al were used, as implemented in the molecular simulation software TREMOLO-X,[55] and have been successfully applied in the MD simulations of silicic acid oligomerization.[51,52,56,57] Reactions between different molecules involved the formation of water when exterior OH groups reacted, and the molecules polymerized in a typical condensation reaction. For instance, a basic reaction between monomers was the following, where two hydroxyls reacted to form water and a bridging O atom

$$2Si(OH)_4 \rightarrow Si_2O(OH)_6 + H_2O \quad (3)$$

The FG potential is composed of two-body and three-body potentials as follows[58]

$$V(\{\mathbf{R}_i\}) = \sum_{i,j} V_2(\mathbf{r}_i, \mathbf{r}_j) + \sum_{i,j,k} V_3(\mathbf{r}_i, \mathbf{r}_j, \mathbf{r}_k) \quad (4)$$

where $V(\{\mathbf{R}_i\})$ is the total potential, in which $\{\mathbf{R}_i\} = (\mathbf{r}_1, \mathbf{r}_2, ..., \mathbf{r}_N)$ are the coordinates for an $N$-atom system. The modified Born−Mayer−Huggins potential is used to represent the interactions between two atoms (e.g., atoms $i$ and $j$). The Rahman−Stillinger−Lemberg (RSL2) potential was used to describe the interactions between hydrogen and the other atoms (e.g., O, Si, Al, or Na) in the modeling system. During the dimerization of aluminate and silicate monomers and the oligomerization of clusters, all of the oxygen atoms are treated as interchangeable with the RSL2 potential,[58] so they can dissociate and form water.

The three-body term in the right-hand side of eq 4 was developed by Stillinger and Weber for their effective silicon potential.[59] All of the values of the constants in the above equations and more details about the FG potential are available in the articles by Feuston and Garofalini.[50,58]

*2.1.2. MD Simulation Models.* The models for our geopolymerization simulations are summarized in Table 1, with the temperature schemes applied during the respective simulations. These models were created with Si/Al ratios of 2 and 3 (designated models M2 and M3) to investigate the influence of Si/Al ratio on the reaction kinetics. The density for the simulation models was 1.32 g/cm$^3$ with cubic simulation boxes whose sizes are shown in Table 1. The simulations contained 144 $Si(OH)_4$ and 72 $NaAl(OH)_4$ in the M2 models, and 150 $Si(OH)_4$ and 50 $NaAl(OH)_4$ in the M3 models. An optimization of the molecular geometry and simulation domain size at 0 K was carried out first using the modified conjugated gradient method by Polak−Ribiére.[60] The model system was then heated up to 300 K to randomize the molecules for 1 ps and then further heated up to the respective "highest temperature" (e.g., 650, 1000, 1200, 1500, and 1800 K for schemes a, b, c, d, and e) for polymerization (as shown in Table 1).

**Table 1. Detailed Information of the MD Simulation Models**

| [a] model | Si/Al ratio | number of monomers | cube length (Å) | density (g/cm$^3$) |
|---|---|---|---|---|
| M2a, b, c, d and e | 2 | $Si(OH)_4$:144 $NaAl(OH)_4$: 72 | 30.5 | 1.32 |
| M3a, b, c, d and e | 3 | $Si(OH)_4$:150 $NaAl(OH)_4$: 50 | 29.5 | 1.32 |

[b] Temperature Scheme

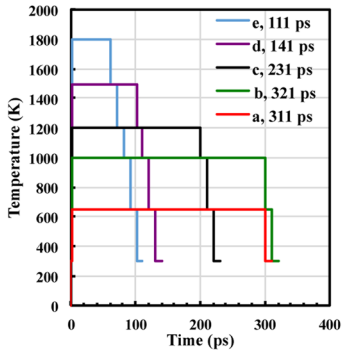


[a] Two different Si/Al ratios were considered (Si/Al = 2, or the M2 model; Si/Al = 3 or the M3 model). Different peak temperatures were used, as designated by a, b, c, d, and e (650, 1000, 1200, 1500, and 1800 K, respectively). [b] The graphical summary is given to show the heating/cooling schemes of the simulation.

The Si and Al sites, in terms of $Si_n$ and $Al_n$, were evaluated to examine the degree of oligomerization. The $Si_n$ and $Al_n$ parameters are semiequivalent to the $Q_n$ parameter (often identified through NMR studies), which are tetrahedral silicates and aluminates connected to $n$ bridging oxygen atoms ($n$ = 0−4) and (4 − $n$) nonbridging oxygen atoms, respectively, as described by Engelhardt et al.[61] For example, $Si_1$ is a Si atom coordinated to four O atoms, one of which is bridging, meaning that the O atom is bonded to two nonhydrogen atoms (i.e., T−O−T, where T = Si or Al). Once the $Q_n$ reached a constant number within a reasonable timeframe, the system was gradually cooled down to 300 K. The "cooling down" procedures were different depending on the specific temperature schemes (see Table 1). The simulation time at each respective temperature step during the "cool down" process (e.g., 1500, 1200, 1000, 650, and 300 K for the simulations that peaked at 1800 K) was 10 ps to ensure the model to reach equilibrium because the sudden cooling down may cause depolymerization or other structural changes. A summary of the different models and temperature schemes is given in Table 1. Depending on the different total run times shown in Table 1, it took approximately 100−300 h to finish the simulations for different models. After the simulations, water molecules were excluded from all of the models and then the models were optimized at 0 K. The bulk density of these optimized aluminosilicate molecules was estimated to approximately



DOI: 10.1021/acs.jpcc.8b00697
J. Phys. Chem. C 2018, 122, 6760−6773

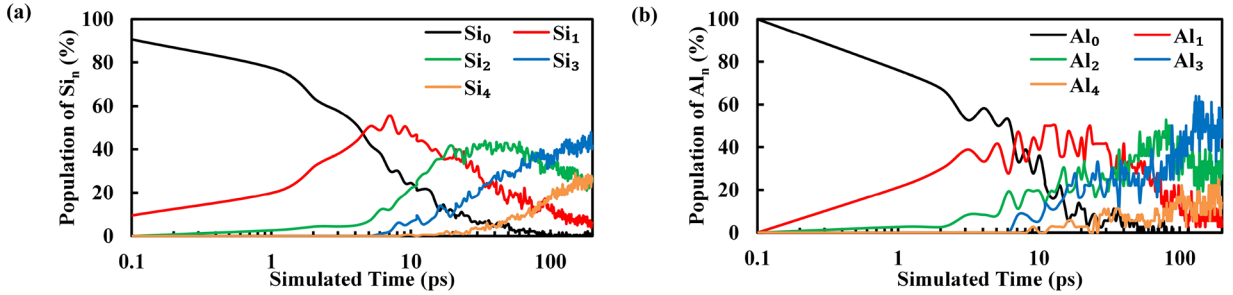


**Figure 1.** Development of $Q_n$ sites for (a) Si and (b) Al in the simulation of aluminosilicates with a Si/Al ratio of 5 at 650 K.

predict the density of geopolymer gels, which include pores and cavities left by the condensation and water extraction.

The temperature was ramped up or down at a rate of 0.5 K/step with a simulation time step of 0.1 fs. Each heating/cooling step was ran until the equilibrium was reached, which is why different simulation time durations were used for different temperature steps. The NVT ensemble was used with a Verlet propagator and a Berendsen thermostat. The entire synthesis process in physical experiments at room temperature (around 300 K), from the mixing of raw materials to the final hardening of geopolymers, usually takes several hours to weeks, depending on the synthesis conditions, whereas the time scale in molecular modeling is on the order of hundreds of picoseconds. Therefore, as a commonly used practice, using higher temperatures in MD simulations is necessary for increasing the reaction rate. In the previous molecular modeling of the polymerization of silicic acid, a high temperature of 2500 K was used to increase the polymerization rate.[52] In the current study, a temperature range of 650−1800 K was used to increase the reaction rate and simulate the experimental effect of "curing temperatures" on the polymerization of geopolymers.

Si/Al ratios in real geopolymers are in the range of 1−3, which is the focus of this paper. Nonetheless, we have also run test simulations with a Si/Al ratio of 5 (Section 3.1) to directly compare with previous published works. The applicability of the reactive FG potential on aluminosilicate molecular systems was verified by comparing our results with the simulations of silicic acid by Garofalini and Martin[51] and Rao et al.[52] These simulations examined the polymerization of silicic acid with 216 $Si(OH)_4$ and 729 $Si(OH)_4$ groups at a density between 1.0 and 1.6 g/cm$^3$ [51,52] and showed appreciable polymerization of those models. We used similar parameters (e.g., 180 $Si(OH)_4$ and 36 $NaAl(OH)_4$ at a density of 1.33 g/cm$^3$) for these calculations (Si/Al = 5). These trial simulations verified (as discussed in Section 3.1) that our approach of using the FG potential for modeling polymerization reactions of aluminosilicates is appropriate.

We characterized the polymerization process by several parameters. The development of $Q_n$ ($Si_n$ and $Al_n$) sites, which is an indicator of the degree of polymerization for aluminosilicate systems, was monitored during the simulation. Because Si and Al atoms are all coordinated with four oxygen atoms in geopolymeric materials and the FG potential used herein was developed to describe four-coordinated Si and Al, the models only contain four-coordinated $Q_n$ sites. Among the five types of four-coordinated Si ($Si_0$, $Si_1$, $Si_2$, $Si_3$, and $Si_4$), $Si_4(m\mathrm{Al})$ (where $m$ is the number of Al linked to $Si_4$ through a bridging O atom) can be quantified with NMR spectra.[35,62,63] Thus, the development of $Si_4(m\mathrm{Al})$ was also monitored during the simulation and compared to the experimental data reported in the literature. The T−O−T (T being Si or Al) bonds were also counted to elucidate the polymerization degree of the models. The degree of condensation, $C$, of each simulation model was calculated using the following equation, which is modified from the degree of condensation for silicic acid models[64]

$$C = \left(\frac{1}{f}\right)\left(\frac{1}{X}\sum_{m=0}^{f} mq_m + \frac{X-1}{X}\sum_{n=0}^{f} nq_n\right) \quad (5)$$

where $f$ is the coordination number for the Si and Al atoms; $m$ and $n$ are the numbers of bridging oxygen connected to an Al center and a Si center, respectively, which range from 0 to 4; $X$ is the Si/Al molar ratio; and $q_m$ and $q_n$ are the fractions of $Al_m$ and $Si_n$, respectively. We only used $f = 4$ to calculate the degree of condensation because all of the Si and Al atoms are four-coordinated in this case due to the nature of the FG potential. The snapshots and the radial distribution functions (RDFs) of the MD models at representative simulation time steps were obtained with the visualization software VMD[65] and compared to the experimental data from X-ray/neutron PDF tests reported in the literature.

## 3. RESULTS AND DISCUSSION

**3.1. Verification of Our Approach.** We first present the results of the trial simulations to verify the feasibility of our approach (Section 2.1) to model polymerization of aluminosilicate systems by comparing with previous simulation work on polymerization of silicic acid[51,52] because the basic reaction mechanism was similar between our simulation and the former work. The polymerization process of the aluminosilicate model is demonstrated by the development of $Q_n$ sites in Figure 1 from the simulation with Si/Al = 5 and ran at 650 K. Both Si and Al sites were considered, designated by $Si_n$ and $Al_n$, respectively. As shown in Figure 1a, the development trend of $Si_n$ is similar to that of the silicic acid system.[58] We also ran simulations for a pure silicate system (not shown) and found similar results to those in the previous simulations.[51] $Si_0$ started to decrease from the very beginning of the simulation, and the other $Si_n$ sequentially increased in the order of $Si_1$, $Si_2$, $Si_3$, and $Si_4$. The Al sites developed in a similar way, although with more fluctuation, as plotted in Figure 1b. The change in the $Q_n$ values for both Si and Al illustrates the polymerization of the silicate and aluminate monomers, which verified the feasibility of FG potential for the simulation of geopolymerization. In the simulation of silicic acid by Garofalini and Martin,[51] the final $Q_n$ ($Q_n$ = Si in their simulations) distribution was 16, 8, 20, 32, and 24% for $Q_0$, $Q_1$, $Q_2$, $Q_3$, and $Q_4$, respectively. Herein, the final distribution was 1, 5, 34, 29, and 34% for $Si_0$, $Si_1$, $Si_2$, $Si_3$, and $Si_4$, and 0, 2, 30, 28, and 12% for $Al_0$, $Al_1$, $Al_2$, $Al_3$, and $Al_4$, respectively. Similarly, $Q_2$, $Q_3$, and $Q_4$ are the dominant sites in



DOI: 10.1021/acs.jpcc.8b00697
J. Phys. Chem. C 2018, 122, 6760−6773

the final systems, regardless of the model or the type of the coordination center (Si or Al). The distribution of $Q_n$ sites in our work is similar to the study by Garofalini and Martin.[51] This comparison was qualitative because our work involved 180 $Si(OH)_4$ and 36 $NaAl(OH)_4$ monomers, whereas Garofalini and Martin's work[51] involved 216 $Si(OH)_4$ monomers. Nonetheless, we see similar trends between two studies: $Si_0$ decreased, whereas $Si_n$ gradually increased in the order of $Si_1$, $Si_2$, $Si_3$, and $Si_4$.

**3.2. Polymerization of Aluminosilicate Precursor.** We then present an overview of our results of the simulations summarized in Table 1. Systems of silicate and aluminate monomers at Si/Al ratios of 2 and 3 were simulated at 650 K following the thermal scheme "a" shown in Table 1. After the simulation at 650 K for 200 ps, almost all of the Si and Al sites were still $Q_0$. For M2a, the final concentrations of $Si_0$ and $Al_0$ were 95.14 and 91.67%, respectively, and those for M3a were 98.67 and 100%, respectively. The final degrees of condensation for M2a and M3a were 1.5 and 0.25%, respectively. The simulation systems barely showed any polymerization or any tendency to polymerize within a reasonable timeframe at 650 K. For other simulation schemes with higher simulation temperatures, the development of $Q_n$ exhibited an apparent polymerization tendency and equilibrated within a reasonable timeframe (ca. 100−300 h, depending on the respective simulation time periods). Because $Si_n$ and $Al_n$ reached equilibrium at different times depending on the initial Si/Al ratios and simulation temperatures, for the different models, $Q_n$ reached equilibrium at the following simulation times: 294 ps for M2b (Si/Al = 2, 1000 K), 273 ps for M2c (Si/Al = 2, 1200 K), 91 ps for M2d (Si/Al = 2, 1500 K), and 55 ps M2e (Si/Al = 2, 1800 K); 292 ps for M3b (Si/Al = 3, 1000 K), 272 ps for M3c (Si/Al = 3, 1200 K), 96 ps for M3d (Si/Al = 3, 1500 K), and 54 ps M3e (Si/Al = 3, 1800 K). Although the polymerization rates and degrees of these models were dependent on the simulation temperature and Si/Al ratio, the molecules were polymerized in a similar trend. Thus, only the results of molecular structures, represented by $Q_n$ ($Si_n$ and $Al_n$), degree of condensation, and RDF, in the model M2e with a Si/Al ratio of 2 simulated at 1800 K are presented in this section for briefness. The effect of simulation temperature and Si/Al ratio on the polymerization is discussed in the following sections.

*3.2.1. $Q_n$ Distribution.* As shown in Figure 2, $Si_1$ and $Al_1$ started to grow immediately as the simulations began, with a concurrent decrease of $Si_0$ and $Al_0$. The concentrations of $Si_1$ and $Al_1$ exceeded those of $Si_0$ and $Al_0$ at 1.5 ps. As expected, $Q_2$ started to form later than $Q_1$. Although the concentration of $Si_2$ exceeded that of $Si_1$ at 8.5 ps, $Al_2$ concentration exceeded $Al_1$ concentration at 15 ps. $Q_3$ and $Q_4$ started to form subsequently, whereas $Q_1$ started to decrease around 2 ps. Finally, $Si_4$ and $Al_4$ reached steady state near 55 and 52 ps, respectively. For the polymerized models simulated at 1800 K (M2e and M3e) after 110 ps, the most populated $Q_n$ sites were $Q_3$ and $Q_4$, whereas for the other models, M2(or 3)b, M2(or 3)c, and M2(or 3)d, which were simulated at 1000, 1200, and 1500 K, respectively, the most populated $Q_n$ sites were $Q_2$ and $Q_3$. This agrees well with the NMR studies reported in the literature, where the experimentally synthesized geopolymer gels were confirmed to be composed of various proportions of $Si_1$, $Si_2$, $Si_3$, and $Si_4$ and the most prevalent ones are $Si_2$ and/or $Si_3$.[66,67] The formation of larger $Q_n$ sites (e.g., $Q_3$ and $Q_4$) at later stages elucidates that the polymerization between small clusters composed of $Q_0$, $Q_1$, and $Q_2$ is the essential reaction pathway to the condensation. It should be noted that the fluctuation of the $Q_n$ distribution curves might be caused by the interchanging among different $Q_n$ sites. For instance, $Q_4$ species may react to form $Q_3$ species because $Q_3 \leftrightarrow Q_4$ is reversible. These interchanges continuously occurred due to reorganization of molecular structures, such as ring opening, ring forming, and cluster−cluster aggregation, during the polymerization process. This is consistent with the simulation study on silicic acid polymerization.[64,68]

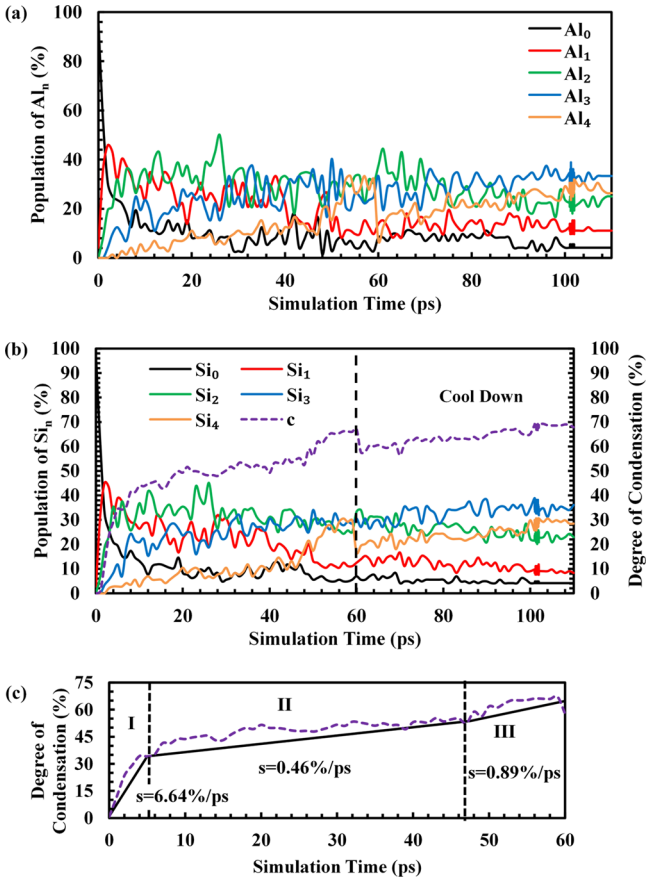


**Figure 2.** Development of (a) $Al_n$ and (b) $Si_n$ and the degree of condensation in the model with Si/Al = 2 at 1800 K (M2e), with the three stages of polymerization before the cool down process enlarged in (c). Note *s* is the average slope for the curve of the degree of condensation at each of the three stages.

To further illustrate the reaction rate of the models, the activation energy was estimated for each $Q_n$ species of the models with Si/Al = 2 and Si/Al = 3. The reaction rate of each $Q_n$ species was approximated by the average increasing slope of the $Q_n$ distribution curves. The reaction rates and the corresponding temperatures were plotted as the $\ln k$ versus $\frac{1}{T}$ curves for each $Q_n$ species of the M2 and M3 models according to the rearranged Arrhenius equation $\ln k = \ln A - \frac{E_a}{R}\cdot\frac{1}{T}$. Through regression analysis of the $\ln k$ versus $\frac{1}{T}$ curves, the activation energies $E_a$ of all of the $Q_n$ sites were estimated, as shown in Table 2.

*3.2.2. Degree of Condensation and Molecular Structures during Simulations.* The degree of condensation, *C*, was calculated on the basis of the population of $Q_n$ and is plotted with simulation time in Figure 2b. The increasing trend in the



DOI: 10.1021/acs.jpcc.8b00697
J. Phys. Chem. C 2018, 122, 6760−6773

Table 2. Approximated Activation Energy of the $Q_n$ Sites for the Models with Si/Al = 2 and 3 Based on Arrhenius Equation

| $E_a$ (kcal/mol) | $Si_1$ | $Si_2$ | $Si_3$ | $Si_4$ | $Al_1$ | $Al_2$ | $Al_3$ | $Al_4$ |
|---|---|---|---|---|---|---|---|---|
| M2 (Si/Al = 2) | 21.5 | 12.9 | 7.7 | 18.2 | 21.5 | 19.2 | 16.9 | 16.7 |
| M3 (Si/Al = 3) | 22.6 | 16.1 | 19.5 | 4.4 | 20.4 | 19.2 | 14.4 | 12.7 |

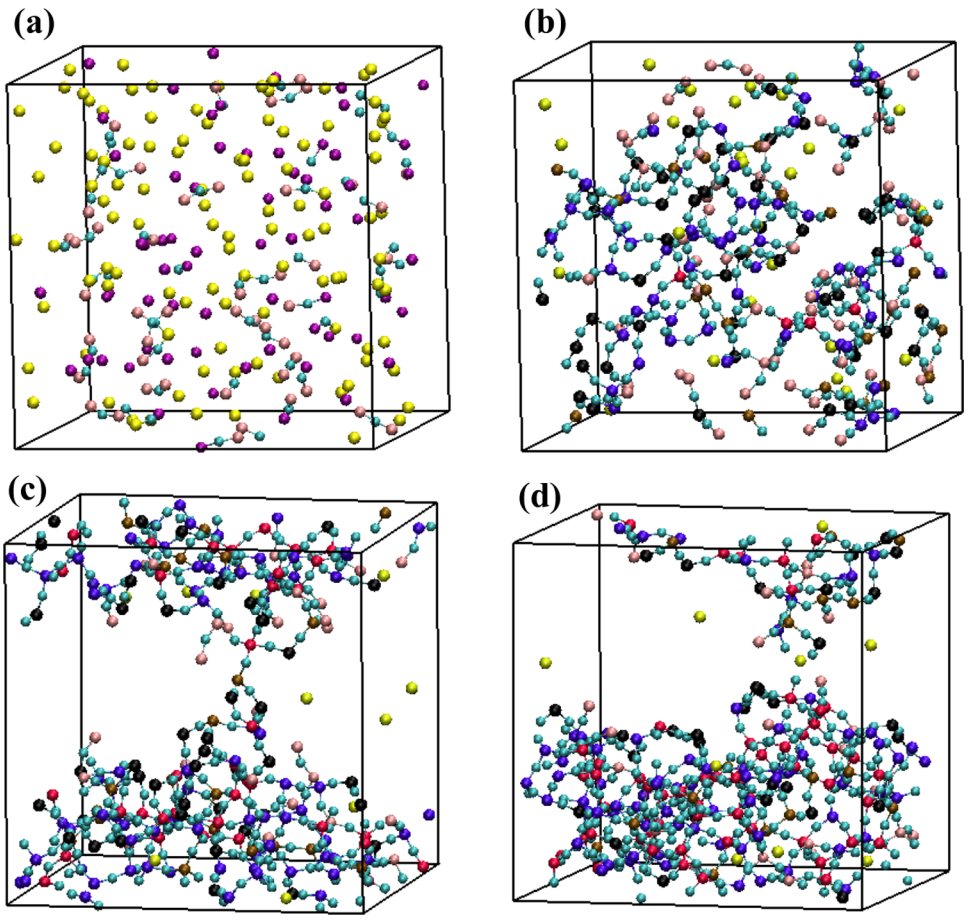


**Figure 3.** Snapshots of the molecular structures in M2e at (a) 1 ps, (b) 10 ps, (c) 50 ps, and (d) 110 ps (after cooling) during the simulation. The color coding is as follows: red, $Q_4$; violet, $Q_3$; black, $Q_2$; pink, $Q_1$; yellow, $Q_0$; and cyan, bridging oxygen. The nonbonded oxygen, terminal oxygen, and all of the hydrogen atoms are excluded for clarity.

degree of condensation suggests that the silicate and aluminate monomers polymerized into a more condensed network gradually. On the basis of the average slope, *s*, of the curve for *C* in Figure 2c, the entire polymerization process can be divided into three stages: (I) oligomerization, (II) aggregation, and (III) condensation. Similar stages have been identified in previous works involving silica systems.[64,68] It should be noted that the slopes representing the reaction rates are only used for categorizing the different polymerization steps, and no experimental results exist for comparison. The slopes of the degree of condensation curve for these three stages are 6.64, 0.46, and 0.89%/ps, respectively. The boundaries between two consecutive polymerization stages are 5 and 47.5 ps, respectively, which correspond to the time instants when $Si_2$ exceeds $Si_0$, and $Si_3$ and $Si_4$ exceed $Si_1$ and $Si_2$, as demonstrated in Figure 2b. $Si_2$ is the main component in the chain structures and single-ring clusters, whereas $Si_0$ and $Si_1$ are the characteristic coordinations in small oligomers. Therefore, the change in the $Si_n$ coordination at the first-stage boundary illustrates the formation of a large number of ring structures. The change in $Si_n$ at the boundary between stage II and III indicates the condensation of the ring clusters because $Si_3$ and $Si_4$ represent the cross-linked tectosilicate frameworks.

These three stages have been qualitatively verified with snapshots of the molecular structures during the simulations. Molecular configurations of the model (M2e) at 1, 10, 50, and 110 ps, which are within stage I, II, III, and the "cool down" process, respectively, are presented in Figure 3. To show the essential framework of the models, the nonbonded oxygen, terminal oxygen, and all of the hydrogen atoms were excluded in the snapshots for clarity. At stage I (Figure 3a), almost all of the Si and Al are $Q_1$ and $Q_0$ with a small amount of $Q_2$. At this stage, because of the high concentration of hydroxyl groups, silicate and aluminate monomers collided frequently and then they dimerized to form small oligomers. Therefore, $Q_0$ decreased, whereas $Q_1$ and $Q_2$ increased rapidly. Subsequently, the increasing concentration of these small oligomers enhanced the probability of polymerization and thus $Q_3$ increased and $Q_1$ decreased (Figure 3b). The formation of ring structures started at stage II, as illustrated in Figure 3b. At stage III (Figure 3c), the small oligomers polymerized into relatively large clusters via cross-linking activities, illustrated by the large number of formed $Q_4$ (Figure 3c), with $Si_4$ increasing from 10 to 28% at



DOI: 10.1021/acs.jpcc.8b00697
J. Phys. Chem. C 2018, 122, 6760−6773

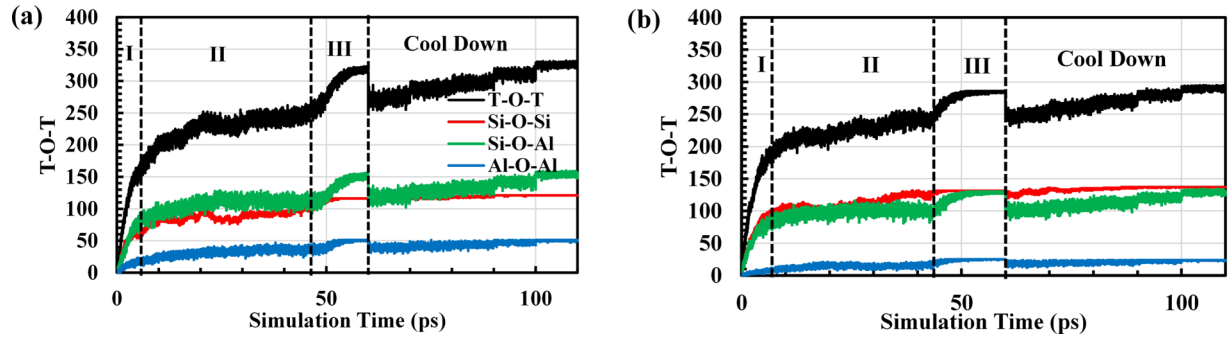


**Figure 4.** Development of T−O−T bonds (T = Si, Al) during the simulations with Si/Al ratios of (a) 2 (M2e) and (b) 3 (M3e). Results are from the simulations with a highest temperature of 1800 K. The quantity of T−O−T is the sum of the three bond types: Si−O−Si, Si−O−Al, and Al−O−Al.

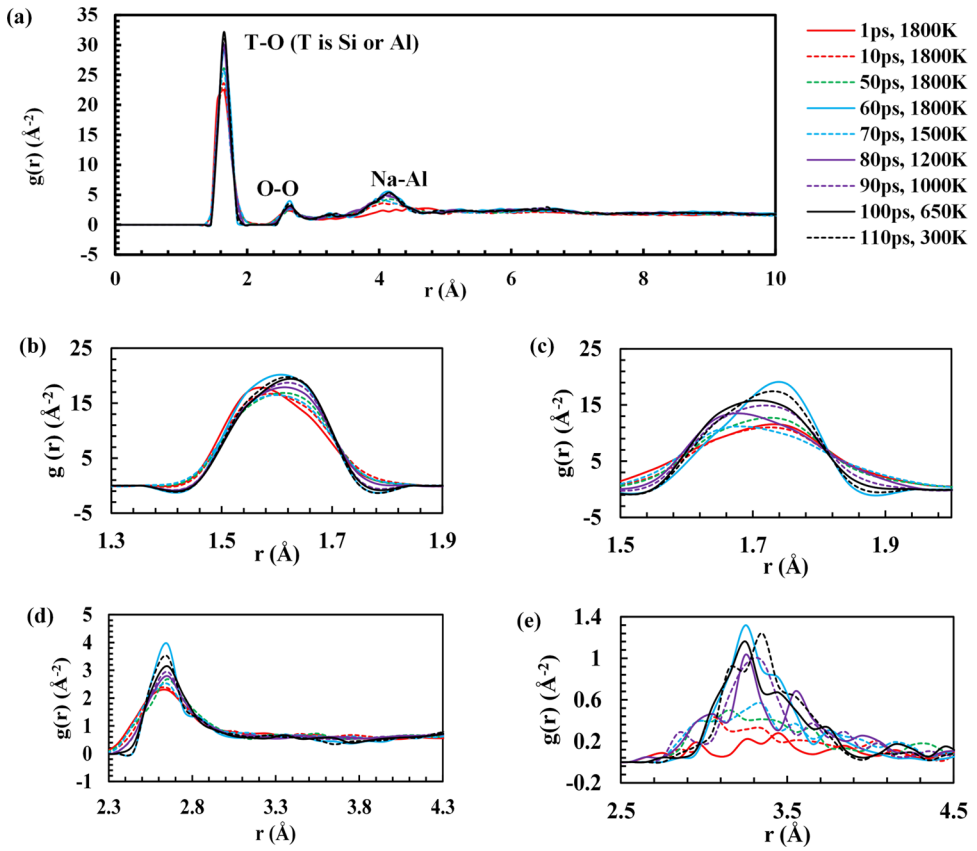


**Figure 5.** Radial distribution functions (RDFs) of the results with a Si/Al ratio of 2 and highest temperature of 1800 K (M2e) at various time instants during simulation. (a) The superimposed RDF for atom pairs, (b) Si−O correlation, (c) Al−O correlation, (d) O−O correlation, and (e) Na−Al correlation.

this stage. The change in molecular structure throughout the first two stages well represented the reaction process from reactive silicate and aluminate monomers to aluminosilicate polymers that consisted of oligomers in different sizes, whereas stage III is consistent with the process from aluminosilicate polymers to geopolymer gels in the conceptual reaction process[38] (eq 2). The sudden decrease in temperature at the start of the "cool down" process (Figure 3e) slightly reduced the condensation degree due to the temporary decrease of large $Q_n$ (e.g., $Q_3$ and $Q_4$). Meanwhile, the concentration of the small $Q_n$ increased, implying that some small clusters, such as monomers and dimers, were disassociated from the main molecular network. Along the cooling process, the simulation system reorganized and those small clusters were reincorporated to the network. Therefore, the final condensation degree and molecular structure are similar to those before cooling, as shown in Figures 2 and 3c,d, respectively.

*3.2.3. Development of T−O−T Bonds.* As another main indicator of geopolymerization, the distribution of T−O−T (T: Si or Al) bonds in the model with Si/Al ratios of 2 and 3 at 1800 K (M2e and M3e) is plotted as a function of simulation time in Figure 4. The number of Si−O−Si, Si−O−Al, and Al−O−Al bonds, along with their sum (the number of T−O−T bonds), increased during the simulation in both M2e and M3e models. Before the models were cooled down to lower temperatures, the T−O−T bonds were equilibrated around 52 and 48 ps with final numbers of bonds of 327 and 288 in models M2e and M3e, respectively. It is reasonable that the T−



DOI: 10.1021/acs.jpcc.8b00697
J. Phys. Chem. C 2018, 122, 6760−6773

O−T bonds in the M3e model were fewer than those in the M2e model because there are fewer monomers in the initial model of M3e compared to M2e to keep the initial density of the models consistent, as detailed in Table 1. Once the simulation temperature started to decrease at the cooling down stage, the number of T−O−T bond structures reduced immediately, mainly due to the breaking of some Si−O−Al bonds that are weaker than the Si−O−Si bonds.[69] However, at the end of the cooling process, the number of Si−O−Al and T−O−T bonds increased and equilibrated to a level similar to that before the cooling. In the M2 model series (e.g., M2b, M2c, M2d, and M2e), Si−O−Si bonds were always fewer than Si−O−Al because the dimerization between a Si monomer and an Al monomer is more preferable than that between two Si monomers, as illustrated by Yang et al. in their study.[46] However, Si−O−Si bonds were always slightly more than the Si−O−Al bonds in the M3 model series (e.g., M3b, M3c, M3d, and M3e) due to a relatively higher Si/Al ratio than the M2 models. Although Al−O−Al bonds increasingly formed during the simulation, their number is still much fewer than the other T−O−T bonds in each model and even more limited in the M3e model. The small number of Al−O−Al bonds formed during the simulations is consistent with the findings in a previous $^{29}$Si NMR study of geopolymers, which illustrated that Loewenstein's rule of aluminum avoidance may not be strictly applied to geopolymer gels.[35] In addition, Al−O−Al bonds equilibrated at final concentrations of 2.2, 6.8, 9.2, and 10.9% in the models with a Si/Al ratio of 2 were simulated at 1000, 1200, 1500, and 1800 K, respectively. The increasing trend in the number of Al−O−Al bonds with temperature implies that more energy input may allow the formation of more Al−O−Al bonds. The increase in T−O−T bonds demonstrates that the aluminosilicate networks were gradually formed through the polymerization of the dispersed silicate and aluminate monomers along the simulation. The T−O−T bonds of the M2e system increased the fastest during stage I due to the oligomerization process, consistent with the condensation process shown in Figure 2c. They subsequently increased more slowly during stage II as the dominant ring-closing and aggregation processes during this stage would not introduce a very large change in T−O−T bonds. During stage III, the T−O−T bonds increased faster than that during stage II because the condensation process involves a high degree of cross-linking reactions, which increased T−O−T bonds, as depicted in Figure 4a. A similar trend is also observed in the development of T−O−T bonds shown in Figure 4b for model M3e.

*3.2.4. Radial Distribution Functions.* The radial distribution functions (RDFs) for Si−O, Al−O, O−O, and Na−Al from the results of the M2e model are superimposed and presented in Figure 5 at various time instants of the polymerization process. After the polymerization at 1800 K for 60 ps, the model was cooled down through the simulation in several steps to 300 K (i.e., 1800 > 1500 > 1200 > 1000 > 650 > 300 K), as shown in Table 1. At each cooling temperature, the simulation lasted 10 ps. Therefore, the RDFs at 70, 80, 90, 100, and 110 ps are plotted to reveal any change in the molecular structure during the cooling process. There is no long-term order in the structures, indicating the amorphous nature of the molecular system. For M2e model at 1800 K, the r(Si−O) (Figure 5b) was centered at 1.55 Å after the simulation of 1 ps and then shifted to 1.6 Å. From 1 to 50 ps, r(Si−O) was centered at 1.6 Å with similar intensities. The bandwidth and intensity increased from 50 to 60 ps. After the temperature decreased from 1800 to 1200 K (60−80 ps), the intensity of r(Si−O) decreased. During the subsequent cooling process, the band for r(Si−O) slightly narrowed with its center shifting to a higher number, which was around 1.64 Å, and its intensity gradually increased back to the level at 60 ps (i.e., before the cooling). The band of r(Al−O) was less symmetric and wider than that of r(Si−O), as presented in Figure 5c. From 1 to 50 ps, the r(Al−O) was centered at 1.75 Å and gradually increased onward. The band intensity significantly increased from 50 to 60 ps and immediately decreased and shifted to 1.65 Å after the temperature reduced at the beginning of the cooling process. The band of r(Al−O) increased back to the intensity before the cooling, similar to r(Si−O), and was centered at 1.75 Å. The changes in r(Si−O) and r(Al−O) during the simulation are consistent with the development of Si−O−Al bond and the degree of condensation, as shown in Figures 4a and 2b, respectively. During the polymerization and condensation of the model at 1800 K, the bonds of Si−O and Al−O in monomers were converted to more polymerized forms in geopolymer gels and then reorganized and stabilized during the condensation process when the model gradually cooled down to 300 K. The RDF development of Si−O and Al−O from the MD simulations agrees well with the experimental results of (Si, Al)−O determined with in situ synchrotron X-ray and neutron pair distribution function by White et al.[36,37] The Si−O and Al−O bonds were presented as one single peak in these experimental results in the range of 1.5−1.8 Å. As shown in Figure 5b,c, the center of Si−O and Al−O correlation increased initially and decreased during the cooling down process. This development trend was similar to the trend of (Si, Al)−O correlation in the experimental study by White et al.,[36] which increased initially and decreased after the geopolymer was cured for 90 days. The RDFs of O−O, plotted in Figure 5d with a peak between 2.3 and 2.9 Å, became narrower along the simulation and its intensity developed in a similar trend to r(Si−O). The correlation between Na and Al is shown in Figure 5e, which has multiple peaks before 50 ps. After 60 ps, only one main peak between 3.0 and 3.5 Å remained distinct for r(Na−Al). This indicates the molecular structure developed into a more ordered configuration after the simulation. The data for r(O−O) and r(Na−Al) are also consistent with the experimental PDFs of O−O and T−Na, respectively, reported by White et al.[37] This indicates the validity of our MD model for computationally "synthesized" geopolymer gels.

Overall, the local bond distances between atoms did not change much during the simulations. Rather, the biggest changes of the modeled system can be attributed to structural alteration (e.g., ring formation and agglomeration) that do not result in long-range order in the RDF plots due to the amorphous nature of the modeled geopolymer gels.

**3.3. Effect of Si/Al Ratio on Geopolymerization Process.** Figure 6 shows the development of $Si_4(mAl)$ during the simulations in the models with Si/Al ratios of 2 and 3 at 1800 K (M2e and M3e). Silicon tetrahedral centers $Si_4(0Al)$, $Si_4(1Al)$, $Si_4(2Al)$, and $Si_4(3Al)$ gradually increased during the simulations. The population of $Si_4(mAl)$, as an indicator of the Si−Al interconnectivity, well explains the effect of Si/Al ratio on the polymerization. In general, a higher population of $Si_4$ connecting to fewer Al centers (e.g., $Si_4(0Al)$, $Si_4(1Al)$, and $Si_4(2Al)$) implies a more polymerized molecular structure. In M2e, the population of all of the $Si_4(mAl)$ increased at a low rate in the first 40 ps, except for $Si_4(4Al)$, which is always 0. From 40 to 60 ps, $Si_4(1Al)$ and $Si_4(2Al)$ increased rapidly to



DOI: 10.1021/acs.jpcc.8b00697
J. Phys. Chem. C 2018, 122, 6760−6773

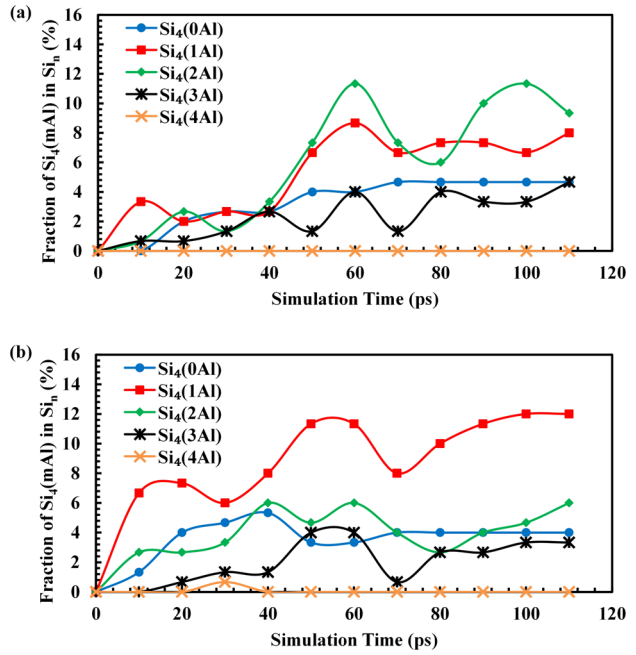


**Figure 6.** Development of $Si_4(mAl)$ as a fraction of Si four-coordinated sites ($Si_n$) in the simulation models with Si/Al ratios of (a) 2 and (b) 3 simulated at 1800 K ($m$ = 0, 1, 2, 3, or 4).

the highest populations. On the other hand, in the M3e model, $Si_4(1Al)$ increased rapidly during the simulation, and $Si_4(0Al)$, $Si_4(2Al)$, and $Si_4(3Al)$ increased at a lower rate, whereas $Si_4(4Al)$ was barely formed during the entire simulation. At the end of the simulations, $Si_4(2Al)$ and $Si_4(1Al)$ are the most populated Si tetrahedral centers in the models with Si/Al ratios of 2 and 3, respectively. This implies that the aluminosilicate systems have been highly polymerized, consistent with the observations in the last section.

The final $Si_4(mAl)$ site distributions of the models simulated at 1800 K are also presented as the fraction of the total amount of $Si_4(mAl)$ in Figure 7, where similar experimental results estimated from the solid-state $^{29}Si$ NMR characterization of geopolymer gels in the literature are also included for comparison. The experimental results by Duxson et al.[35] were obtained from metakaolin-based geopolymers with nominal Si/Al ratios of 1.9 and 2.1, and the results by Fernández-Jiménez et al. and Lyu et al. were obtained from fly ash-based

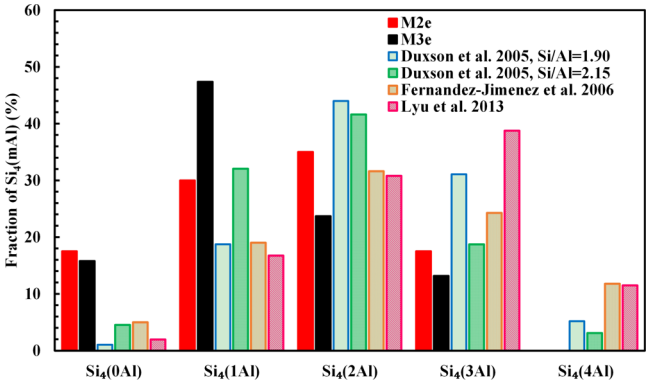


**Figure 7.** Fraction of $Si_4(mAl)$ from the simulations with Si/Al ratios of 2 and 3 at 1800 K. Results are compared with the similar experimental results obtained with $^{29}Si$ NMR.[33−35]

geopolymers.[29,33] The molecular structures generated from the current simulations consist of $Si_4(0Al)$, $Si_4(1Al)$, $Si_4(2Al)$, and $Si_4(3Al)$, where the experimentally synthesized geopolymers in the literature are composed of $Si_4(1Al)$, $Si_4(2Al)$, $Si_4(3Al)$, and $Si_4(4Al)$. Compared to the experimental results, our simulation results have more $Si_4(0Al)$ and $Si_4(1Al)$, but fewer $Si_4(4Al)$. In the NMR study of fly ash-based geopolymers by Lyu et al.,[34] $Si_4(2Al)$ was found dominant in the final distribution of $Si_4(mAl)$ for all of the systems. In the study by Fernández-Jiménez et al.,[33] although the main silicon centers in the fly ash-based geopolymer gels were $Si_4(1Al)$, $Si_4(2Al)$, and $Si_4(3Al)$, there still remained an appreciable portion of $Si_4(4Al)$, which might be due to the relatively short curing period (7 days). The same study showed that for the geopolymers synthesized with the nominal $SiO_2/Na_2O$ ratio of 0−1.17, the percentages of ($Si_4(1Al)$ + $Si_4(2Al)$) and ($Si_4(3Al)$ + $Si_4(4Al)$) were in the ranges of 46−51 and 31−35%, respectively. In the current simulation results plotted in Figure 7, the populations of $Si_4(1Al)$ + $Si_4(2Al)$ and $Si_4(3Al)$ + $Si_4(4Al)$ are in the ranges of 65−71 and 13−18%, respectively. As shown in previous studies,[63,70] there are more $Si_4(3Al)$ and $Si_4(4Al)$ in Al-rich geopolymer gels, which have a lower mechanical strength; $Si_4(1Al)$ and $Si_4(2Al)$ sites are formed at a later stage, and there are more such sites present in Si-rich geopolymer gels that have a higher mechanical strength. This implies that along with the curing time, $Si_4(1Al)$ and $Si_4(2Al)$ sites should gradually increase, as would the mechanical strength of geopolymer gels. Figure 7 indicates that our simulations result in more Si-rich gels compared to the experimentally synthesized geopolymer gels reported in the literature.

The discrepancy that more Si-rich geopolymer gels are formed in our simulation than the experiments might be due to the different starting precursors used in the simulation and experimental systems. In the simulation systems, all of the monomers were reactive, whereas in the experimental systems, the reactive monomers had to be released first from the raw materials that are not fully dissolvable. In addition, the $Si_4(4Al)$ detected in the experimentally synthesized geopolymer samples may be attributed to the residues of the raw materials. Unlike the physical experiments, the geopolymerization process in the simulations is not affected by excessive water content, the degree of dissolution of raw materials, excessive silicate or alkali concentrations, or low temperatures. Therefore, the polymerization degree and the proportion of $Si_4(0Al)$ and $Si_4(1Al)$ of the geopolymer gels in the current simulation study are higher.

As demonstrated in Figure 7, the proportion of $Si_4(1Al)$ in the model with a Si/Al ratio of 2 is lower than that in the model with a Si/Al ratio of 3, whereas the proportions of $Si_4(2Al)$ and $Si_4(3Al)$ are higher in the M2 model series. This trend is consistent with the findings reported in the study by Duxson et al.,[35] where $Si_4(1Al)$ in the geopolymers with a nominal Si/Al ratio of 1.90 was lower compared to a counterpart with a Si/Al ratio of 2.15 and the percentages of the other $Si_4(mAl)$s were higher in the geopolymers with a Si/Al ratio of 1.90. This implies that Si−O−Al bonds in the geopolymer gels decreased with the increase of the nominal Si/Al ratio. The results of the simulation model with a Si/Al ratio of 2 are also qualitatively similar to the NMR results by Duxson et al.,[35] where the proportions of $Si_4(2Al)$ and $Si_4(4Al)$ were the most and the least distributed silicate tetrahedrons, respectively, for the systems with nominal Si/Al ratios of 1.90 and 2.15. This qualitative comparison suggests that (i) the main $Si_4(mAl)$ sites in the current simulated geopolymer systems are $Si_4(1Al)$ and


DOI: 10.1021/acs.jpcc.8b00697
J. Phys. Chem. C 2018, 122, 6760−6773

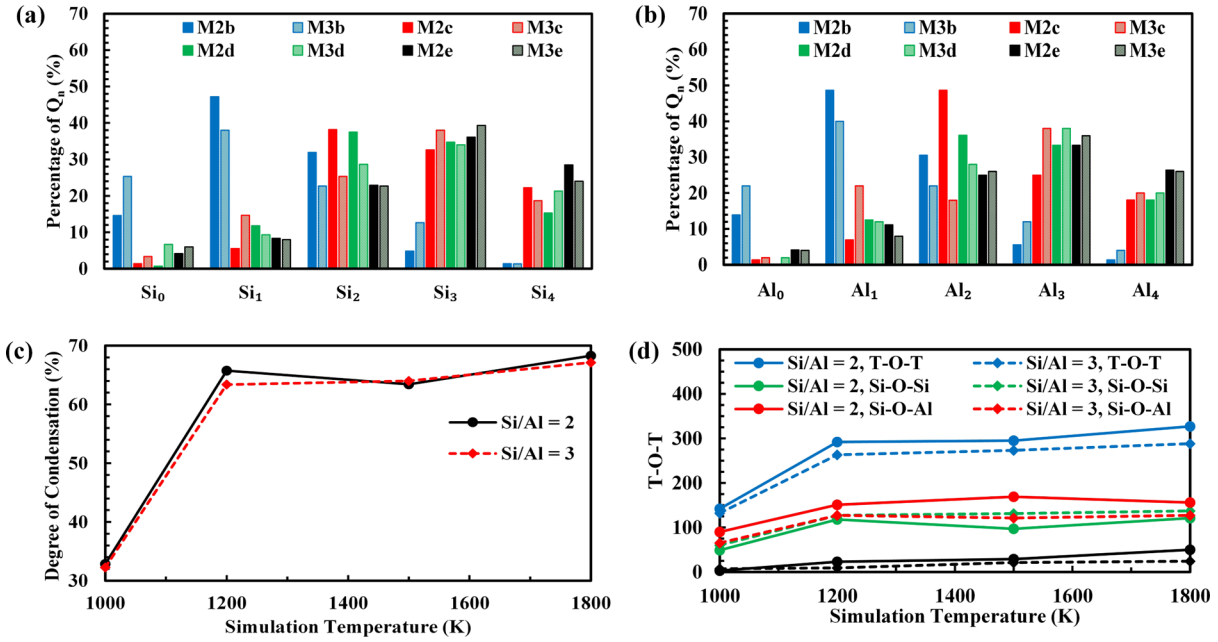


**Figure 8.** Effect of Si/Al ratio on the quantities of (a) $Si_n$, (b) $Al_n$, (c) degree of condensation, and (d) number of T−O−T Bonds. Results are shown for various temperatures.

$Si_4(2Al)$, whose populations are qualitatively consistent with the experimental results in the literature and (ii) the Si/Al ratio plays an important role in the resulting molecular structures of geopolymer gels.

The effect of Si/Al ratio on the polymerization is further explained by the final percentages of $Q_n$, final degrees of condensation, and the final number of T−O−T bonds in Figure 8. As shown in Figure 8a,b, in most of the M2 model series (Si/Al = 2), the final proportions of $Q_0$ and $Q_3$ were lower than those in the M3 model series (Si/Al = 3), but $Q_1$ and $Q_2$ were higher than the M3 counterparts. The dependence of the final proportions of $Si_4$ on Si/Al ratio is different from that of $Al_4$. The final proportions of $Si_4$ in the M2 models at 1000, 1200, and 1800 K were higher than those in the M3 counterparts, whereas the final proportions of $Al_4$ in the M2 models at 1000, 1200, and 1500 K were slightly lower than those in the M3 counterparts. Because Si tetrahedrons are the major components in geopolymeric networks and $Si_4$ represents the degree of polymerization better than $Al_4$, the final molecules of geopolymer gels from the M2 models should be more cross-linked than those from the M3 models in general. Consistently, the degrees of condensation of the M2 models simulated at 1000, 1200, and 1800 K were higher than those of the M3 counterparts (see Figure 8c). As illustrated in Section 3.2, the differences in T−O−T bond developments for the different systems are: (i) the M2 models had more Si−O−Si bonds than Si−O−Al bonds, whereas the M3 models followed the opposite trend and (ii) more Al−O−Al bonds were formed in the M2 models compared to the M3 models. This phenomenon is also illustrated by the number of resulting T−O−T bonds in the final simulation systems at different temperatures, as shown in Figure 8d. More Si−O−Al and Al−O−Al bonds were formed in the resulting molecular models with a Si/Al ratio of 2 than the models with a Si/Al ratio of 3, for all of the simulation temperatures. On the other hand, more Si−O−Si bonds were formed in the models with a Si/Al ratio of 3 than those in the models with a Si/Al ratio of 2. These differences are mainly due to the different Si/Al ratios, where Al−O bonds have a lower probability to form, but it is more likely for Si−O bonds to form in the models with a relatively higher Si/Al ratio. Overall, the simulation results showed similar degrees of polymerization (see Figure 8c) for both Si/Al ratios at each temperature.

**3.4. Effect of Simulation Temperature on Geopolymerization Process.** The fractions of $Si_4(mAl)$ in the final $Si_4$ sites of all of the models simulated at different temperatures are depicted in Figure 9. In the models simulated

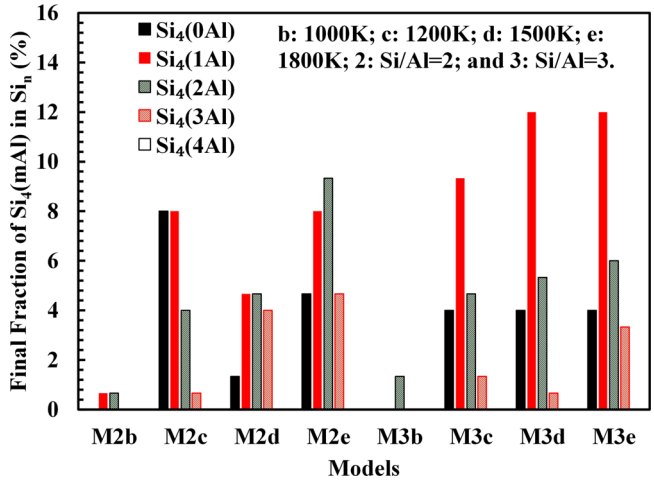


**Figure 9.** Final distribution of $Si_4(mAl)$ in the models with Si/Al ratios of 2 and 3 at temperatures of 1000 K (M2b and M3b), 1200 K (M2c and M3c), 1500 K (M2d and M3d), and 1800 K (M2e and M3e).

at 1000 K (M2b and M3b), only small numbers of $Si_4(1Al)$ and $Si_4(2Al)$ were formed due to the low degree of polymerization. For the models with a Si/Al ratio of 3 (M3 model series), the total $Si_4(mAl)$, $Si_4(1Al)$, and $Si_4(2Al)$ increased with increasing simulation temperatures. For the models with a Si/Al ratio of 2 (M2 model series), $Si_4(2Al)$ and $Si_4(3Al)$ increased with the simulation temperature; the concentrations of $Si_4(0Al)$,


DOI: 10.1021/acs.jpcc.8b00697
J. Phys. Chem. C 2018, 122, 6760−6773

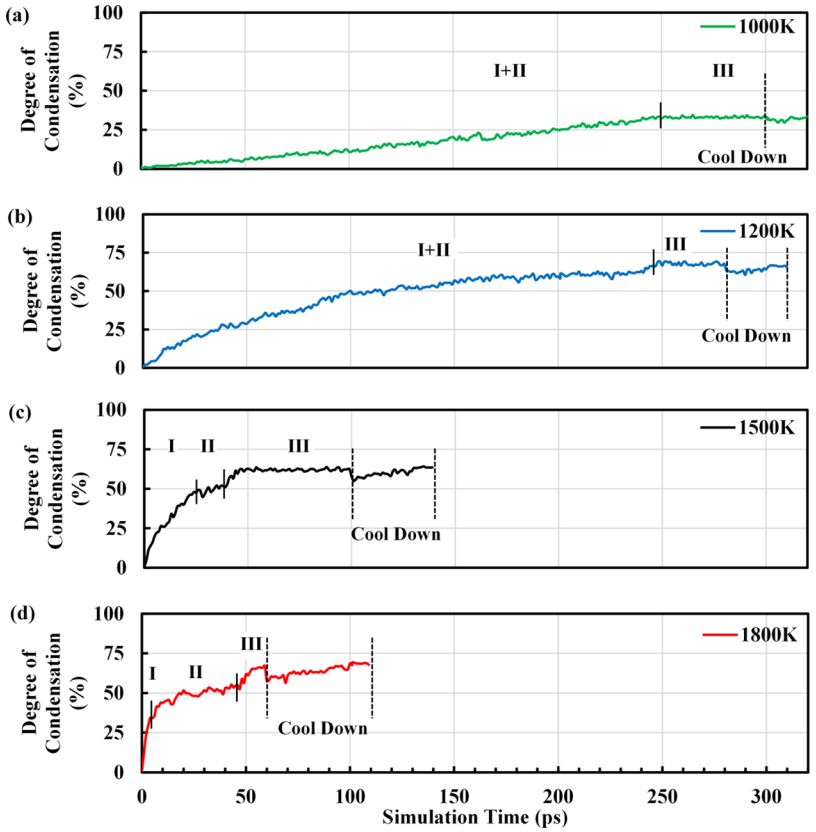


**Figure 10.** Degree of condensation ($C$) for the M2 models (Si/Al ratio of 2) at (a) 1000 K, (b) 1200 K, (c) 1500 K, and (d) 1800 K. Stages I, II, and III are the processes of oligomerization, aggregation, and condensation, respectively.

$Si_4(1Al)$, and $Si_4(2Al)$ in M2d (1500 K) are lower than those in M2c (1200 K) and thus the total $Si_4(mAl)$ in M2d is fewer than that in M2c. As evident from Figure 9, the effect of simulation temperatures on the molecular structures of the models is also intertwined with Si/Al ratio because the development of $Si_4(mAl)$ with simulation temperatures in M2 models is not consistent with that in M3 models. Such intertwining effects of the curing temperature and Si/Al ratio on geopolymerization are also reported in experimental synthesis studies in the literature.[40,71]

The effect of simulation temperature on the polymerization can be further demonstrated by the degree of condensation ($C$), as shown in Figure 10. The degree of condensation for the M3 model series (Si/Al = 3) exhibited a similar dependence on the simulation temperature to that for the M2 counterparts (Si/Al = 2), so only the results from the M2 models are presented. The condensation degree increased with simulation time and reached a steady state near 250, 180, 48, and 52 ps for the models at 1000, 1200, 1500, and 1800 K, respectively. In other words, when higher simulation temperatures were applied, shorter simulation time was required to reach the final degree of condensation. In each of the models, the condensation degree dropped once the temperature started to decrease during the "cool down" process and then increased to a similar level before the cooling. The final degrees of condensation of the M2b, M2c, M2d, and M2e models were 33.3, 65.7, 63.5, and 67.8%, respectively. For the models heated to 1000 and 1200 K (M2b and M2c), no apparent boundary between stage I (oligomerization) and stage II (aggregation) can be found, but stage III (condensation) is distinguishable from the early stages. For the model simulated at 1500 K (M2d), the boundaries between the two consecutive stages are 13 and 35 ps, respectively. A higher simulation temperature resulted in shorter stage I (M2d: 0−13 ps and M2e: 0−5 ps) and stage III (M2d: 35−60 ps and M2e: 47.5−60 ps) but a longer stage II (M2d: 13−35 ps and M2e: 5−47.5 ps), as shown in Figure 10c,d. A higher temperature accelerated the oligomerizaiton process and also increased the oligomerization degree, as the degree of condensation ($C$) value of M2e (67.8%) is higher than that of M2d (63.5%) at the end of stage I. A shorter stage II in M2d compared to M2e might be attributed to fewer oligomers available for the aggregation. Consequently, the final condensation degree of M2e is higher than that of M2d. For the models simulated at 1000 and 1200 K, aggregation of oligomers and cluster−cluster condensation occurred simultaneously with the oligomerization due to the relatively low temperature; thus, the final condensation degrees are relatively low. The slightly higher condensation degree of M2c compared to M2d might be due to much longer simulation time (Table 1). Apparently in Figure 10, the degree of condensation at the same simulation time instant was larger at higher simulation temperatures. This illustrates that elevated temperature can effectively enhance the reaction rate, consistent with the experimental results of previous studies.[72−74]

The bulk densities of the model systems simulated at different temperatures were estimated using the total mass of the atoms in the final model divided by the volume of the simulation domain, as plotted in Figure 11. Free water molecules were excluded from this estimation because water is likely to evaporate during the curing process. The densities of the final models are all lower than the initial density due to the removal of the water molecules that left a large proportion of



DOI: 10.1021/acs.jpcc.8b00697
J. Phys. Chem. C 2018, 122, 6760−6773

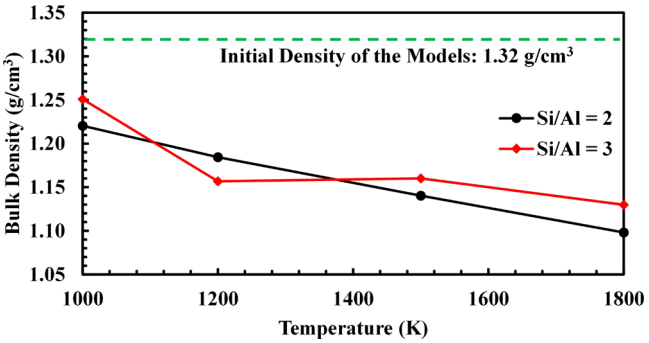


**Figure 11.** Bulk density of the models with Si/Al ratios of 2 and 3. To calculate the density, water formed during polymerization was excluded from the mass of the system (assumed to evaporate).

pores and cavities in the models. The density of the "geopolymer gels" predicted from the simulations is in the range of 1.10−1.25 g/cm$^3$, which is lower compared to the bulk density of metakaolin-based geopolymers, 1.31 g/cm$^3$, experimentally synthesized in a previous study.[75] This discrepancy in the bulk density can be explained by the filling of cavities: cavities in the experimentally synthesized metakaolin-based geopolymers were filled with remaining impurities and unreacted constituents. For both model 2 and model 3 series (with Si/Al ratios of 2 and 3, respectively), their bulk densities decreased with the simulation temperature due to the increasing amount of water exclusion. This agrees well with the effect of curing temperature on the density of geopolymers observed in physical experiments.[22] The density of the polymerized model with a Si/Al ratio of 2 is slightly lower than that of its counterpart with a Si/Al ratio of 3 except for that at 1200 K, implying that (i) the porosity in the M2 models is higher than that in the M3 models and (ii) more water molecules were extracted from the M2 models than those from the M3 models (i.e., more condensation reactions occurred in M2 models). Therefore, the geopolymer frameworks with a Si/Al ratio of 2 were more compact than those with a Si/Al ratio of 3.

## 4. CONCLUSIONS

Reactive MD simulations were performed in this study for the first time to simulate the polymerization process and computationally "synthesize" amorphous geopolymer gels from aluminate and silicate monomers to final geopolymer gels. The influence of simulation temperature and Si/Al ratio on the geopolymerization was evaluated by applying five maximum simulation temperatures from 650 to 1800 K on the models with Si/Al ratios of 2 and 3.

On the basis of the degree of condensation ($C$) and the nature of geopolymerization, the entire polymerization process was divided into three stages, namely, oligomerization, aggregation, and condensation, similar to the polymerization of silica models. During polymerization, the models with dispersed monomers gradually developed into a more condensed and ordered structure. For the first time, geopolymer gels close to the experimentally synthesized ones were computationally simulated, which were qualitatively verified by comparing with NMR and X-ray/neutron PDF results reported in the literature. The good agreement between the current simulation and NMR results in the distribution of $Si_4(mAl)$, which are the $Si_4$ sites that are connected with $m$ Al atoms, indicated that the computationally synthesized geopolymer gels were similar to the experimentally synthesized ones. The RDF patterns for Si−O, Al−O, O−O, and Na−Al atom pairs illustrated the amorphous nature of the simulated molecular structures. These RDF patterns also agreed with the experimental PDF results in the literature, which further confirmed the similarity in molecular structures between the computationally and experimentally synthesized geopolymer gels.

The polymerization process and the properties of the resulting geopolymer gels show apparent dependence on the Si/Al ratio of the initial simulation models. T−O−T bonds, $Si_4$, and degrees of condensation in the models with a Si/Al ratio of 2 are higher than those of their counterparts with a Si/Al ratio of 3, so the molecular structures obtained in the former models are more compact than those obtained in the latter ones. The lower bulk densities of the models with a lower Si/Al ratio implied a higher degree of water formation (monomer reaction) and higher pore volume in the corresponding geopolymeric models. Similar to the experimental observations, both the polymerization rate and the degree of polymerization were accelerated by the increase of temperature. As a result, the bulk density of the resulting geopolymer gels decreased with the increasing simulation temperature. This implies that geopolymer gels cured at a higher temperature tend to have more water evaporated and result in a higher porosity, consistent with the experimental results. The simulation results suggest that a low temperature prolongs the reaction process at the early stage of polymerization and results in a relatively low degree of condensation. This agrees well qualitatively with the experimental findings that reaction rate and degree at low curing temperatures are relatively low. Our results highlight the interplay between temperature and Si/Al ratio on the final geopolymer molecular structure. Furthermore, the molecular structures of the geopolymer gels predicted from the MD simulations in this study can be used for assessing other key properties, such as strength, stiffness, and permeability.

## AUTHOR INFORMATION

### Corresponding Authors

*E-mail: nadeskins@wpi.edu. Phone: 508-831-5445 (N.A.D.).
*E-mail: taomj@wpi.edu. Phone: 508-831-6487. Fax: 508-831-5808 (M.T.).

### ORCID

Mo Zhang: 0000-0001-9680-4203

### Notes

The authors declare no competing financial interest.

## ACKNOWLEDGMENTS

This work was supported by the U.S. National Science Foundation under Grant Nos. CMMI-1301048 and CMMI-1301070. The authors thank the computer support staff at Worcester Polytechnic Institute for their help in using the computer systems. They also thank the TREMOLO-X developers for their help in using the TREMOLO-X code.

## REFERENCES

(1) Davidovits, J. In *Properties of Geopolymer Cements*, First International Conference on Alkaline Cements and Concretes, Oct, 1994; Scientific Research Institute on Binders and Materials, Kiev State Technical University: Ukraine, 1994; Vol. *1*, pp 131−149.

(2) Duxson, P.; Provis, J. L.; Lukey, G. C.; van Deventer, J. S. J. The role of inorganic polymer technology in the development of 'green concrete'. *Cem. Concr. Res.* **2007**, *37*, 1590−1597.



DOI: 10.1021/acs.jpcc.8b00697
J. Phys. Chem. C 2018, 122, 6760−6773

(3) McLellan, B. C.; Williams, R. P.; Lay, J.; van Riessen, A.; Corder, G. D. Costs and carbon emissions for geopolymer pastes in comparison to ordinary Portland cement. *J. Cleaner Prod.* **2011**, *19*, 1080−1090.
(4) Temuujin, J.; Minjigmaa, A.; Rickard, W.; Lee, M.; Williams, I.; van Riessen, A. Preparation of metakaolin based geopolymer coatings on metal substrates as thermal barriers. *Appl. Clay Sci.* **2009**, *46*, 265−270.
(5) Medri, V.; Fabbri, S.; Ruffini, A.; Dedecek, J.; Vaccari, A. SiC-based refractory paints prepared with alkali aluminosilicate binders. *J. Eur. Ceram. Soc.* **2011**, *31*, 2155−2165.
(6) Temuujin, J.; Rickard, W.; Lee, M.; van Riessen, A. Preparation and thermal properties of fire resistant metakaolin-based geopolymer-type coatings. *J. Non-Cryst. Solids* **2011**, *357*, 1399−1404.
(7) Gourley, J. T.; Johnson, G. B. In *Developments in Geopolymer Precast Concrete*, International Workshop on Geopolymers and Geopolymer Concrete; Institut Geopolymere: Perth, Australia, 2005.
(8) Zhang, Z.; Provis, J. L.; Reid, A.; Wang, H. Geopolymer foam concrete: An emerging material for sustainable construction. *Constr. Build. Mater.* **2014**, *56*, 113−127.
(9) Cilla, M. S.; Colombo, P.; Morelli, M. R. Geopolymer foams by gelcasting. *Ceram. Int.* **2014**, *40*, 5723−5730.
(10) Yunsheng, Z.; Wei, S.; Qianli, C.; Lin, C. Synthesis and heavy metal immobilization behaviors of slag based geopolymer. *J. Hazard. Mater.* **2007**, *143*, 206−213.
(11) Malone, P. G.; Randall, C. A., Jr.; Kirkpatrick, T. *Potential Applications of Alkali-Activated Alumino-silicate Binders in Military Operations*, No. WES/MP/GL-85-15; Geotechnical Lab, Army Engineer Waterways Experiment Station: Vicksburg, MS, 1985.
(12) Palomo, Á.; Jiménez, A. F.; Hombrados, C. L.; Lleyda, J. L. Railway sleepers made of alkali activated fly ash concrete. *Rev. Ing. Constr.* **2007**, *22*, 75−80.
(13) Davidovits, J. In *30 Years of Successes and Failures in Geopolymer Applications. Market Trends and Potential Breakthroughs*, Geopolymer 2002 Conference; Geopolymer Institute: Saint-Quentin, France; Melbourne, Australia, 2002; Vol. *28*.
(14) Rowles, M.; O'Connor, B. Chemical optimisation of the compressive strength of aluminosilicate geopolymers synthesised by sodium silicate activation of metakaolinite. *J. Mater. Chem.* **2003**, *13*, 1161−1165.
(15) Barbosa, V. F. F.; MacKenzie, K. J. D.; Thaumaturgo, C. Synthesis and characterisation of materials based on inorganic polymers of alumina and silica: sodium polysialate polymers. *Int. J. Inorg. Mater.* **2000**, *2*, 309−317.
(16) Pacheco-Torgal, F.; Moura, D.; Ding, Y.; Jalali, S. Composition, strength and workability of alkali-activated metakaolin based mortars. *Constr. Build. Mater.* **2011**, *25*, 3732−3745.
(17) Chindaprasirt, P.; Chareerat, T.; Hatanaka, S.; Cao, T. High-Strength Geopolymer Using Fine High-Calcium Fly Ash. *J. Mater. Civ. Eng.* **2011**, *23*, 264−270.
(18) de Vargas, A. S.; Dal Molin, D. C. C.; Vilela, A. C. F.; da Silva, F. J.; Pavão, B.; Veit, H. The effects of $Na_2O/SiO_2$ molar ratio, curing temperature and age on compressive strength, morphology and microstructure of alkali-activated fly ash-based geopolymers. *Cem. Concr. Compos.* **2011**, *33*, 653−660.
(19) Fernandez-Jimenez, A.; García-Lodeiro, I.; Palomo, A. Durability of alkali-activated fly ash cementitious materials. *J. Mater. Sci.* **2007**, *42*, 3055−3065.
(20) Cheng, T. W.; Chiu, J. P. Fire-resistant geopolymer produced by granulated blast furnace slag. *Miner. Eng.* **2003**, *16*, 205−210.
(21) He, J.; Jie, Y.; Zhang, J.; Yu, Y.; Zhang, G. Synthesis and characterization of red mud and rice husk ash-based geopolymer composites. *Cem. Concr. Compos.* **2013**, *37*, 108−118.
(22) Zhang, M.; El-Korchi, T.; Zhang, G.; Liang, J.; Tao, M. Synthesis factors affecting mechanical properties, microstructure, and chemical composition of red mud−fly ash based geopolymers. *Fuel* **2014**, *134*, 315−325.
(23) Songpiriyakij, S.; Kubprasit, T.; Jaturapitakkul, C.; Chindaprasirt, P. Compressive strength and degree of reaction of biomass- and fly ash-based geopolymer. *Constr. Build. Mater.* **2010**, *24*, 236−240.
(24) Brew, D. R. M.; MacKenzie, K. J. D. Geopolymer synthesis using silica fume and sodium aluminate. *J. Mater. Sci.* **2007**, *42*, 3990−3993.
(25) Zhang, L.; Ahmari, S.; Zhang, J. Synthesis and characterization of fly ash modified mine tailings-based geopolymers. *Constr. Build. Mater.* **2011**, *25*, 3773−3781.
(26) Provis, J. L.; Lukey, G. C.; van Deventer, J. S. J. Do geopolymers actually contain nanocrystalline zeolites? A reexamination of existing results. *Chem. Mater.* **2005**, *17*, 3075−3085.
(27) Duxson, P.; Fernández-Jiménez, A.; Provis, J. L.; Lukey, G. C.; Palomo, A.; van Deventer, J. S. J. Geopolymer technology: the current state of the art. *J. Mater. Sci.* **2007**, *42*, 2917−2933.
(28) Rattanasak, U.; Chindaprasirt, P. Influence of NaOH solution on the synthesis of fly ash geopolymer. *Miner. Eng.* **2009**, *22*, 1073−1078.
(29) Lyu, S.-J.; Wang, T.-T.; Cheng, T.-W.; Ueng, T.-H. Main factors affecting mechanical characteristics of geopolymer revealed by experimental design and associated statistical analysis. *Constr. Build. Mater.* **2013**, *43*, 589−597.
(30) Williams, R. P.; Hart, R. D.; van Riessen, A. Quantification of the extent of reaction of metakaolin-based geopolymers using X-Ray diffraction, scanning electron microscopy, and energy-dispersive spectroscopy. *J. Am. Ceram. Soc.* **2011**, *94*, 2663−2670.
(31) Rees, C. A.; Provis, J. L.; Lukey, G. C.; van Deventer, J. S. J. In situ ATR−FTIR study of the early stages of fly ash geopolymer gel formation. *Langmuir* **2007**, *23*, 9076−9082.
(32) Rees, C. A.; Provis, J. L.; Lukey, G. C.; van Deventer, J. S. J. Attenuated total reflectance fourier transform infrared analysis of fly ash geopolymer gel aging. *Langmuir* **2007**, *23*, 8170−8179.
(33) Fernández-Jiménez, A.; de la Torre, A. G.; Palomo, A.; López-Olmo, G.; Alonso, M. M.; Aranda, M. A. G. Quantitative determination of phases in the alkaline activation of fly ash. Part II: Degree of reaction. *Fuel* **2006**, *85*, 1960−1969.
(34) Criado, M.; Fernández-Jiménez, A.; Palomo, A.; Sobrados, I.; Sanz, J. Effect of the $SiO_2/Na_2O$ ratio on the alkali activation of fly ash. Part II: $^{29}Si$ MAS−NMR Survey. *Microporous Mesoporous Mater.* **2008**, *109*, 525−534.
(35) Duxson, P.; Provis, J. L.; Lukey, G. C.; Separovic, F.; van Deventer, J. S. J. $^{29}Si$ NMR study of structural ordering in aluminosilicate geopolymer gels. *Langmuir* **2005**, *21*, 3028−3036.
(36) White, C. E.; Provis, J. L.; Llobet, A.; Proffen, T.; van Deventer, J. S. J. Evolution of local structure in geopolymer gels: An in situ neutron pair distribution function analysis. *J. Am. Ceram. Soc.* **2011**, *94*, 3532−3539.
(37) White, C. E.; Page, K.; Henson, N. J.; Provis, J. L. In situ synchrotron X-ray pair distribution function analysis of the early stages of gel formation in metakaolin-based geopolymers. *Appl. Clay Sci.* **2013**, *73*, 17−25.
(38) Provis, J. L.; van Deventer, J. S. J. Geopolymerisation kinetics. 2. Reaction kinetic modelling. *Chem. Eng. Sci.* **2007**, *62*, 2318−2329.
(39) Provis, J. L.; van Deventer, J. S. J. Direct measurement of the kinetics of geopolymerisation by in-situ energy dispersive X-ray diffractometry. *J. Mater. Sci.* **2007**, *42*, 2974−2981.
(40) Zhang, Z.; Wang, H.; Provis, J. L.; Bullen, F.; Reid, A.; Zhu, Y. Quantitative kinetic and structural analysis of geopolymers. Part 1. The activation of metakaolin with sodium hydroxide. *Thermochim. Acta* **2012**, *539*, 23−33.
(41) White, C.; Bloomer, B. E.; Provis, J. L.; Henson, N. J.; Page, K. L. *The Synergy between Total Scattering and Advanced Simulation Techniques: Quantifying Geopolymer Gel Evolution*, No. LA-UR-11-07026; LA-UR-11-7026; Los Alamos National Laboratory (LANL), 2011.
(42) Zhang, Y.; Wei, S. Semi-empirical AM1 calculations on 6-memebered alumino-silicate rings model: implications for dissolution process of metakaoline in alkaline solutions. *J. Mater. Sci.* **2007**, *42*, 3015−3023.


DOI: 10.1021/acs.jpcc.8b00697
J. Phys. Chem. C 2018, 122, 6760−6773

(43) Zhang, Y.; Jia, Y.; Sun, W.; Zongjin, L. Study of ion cluster reorientation process of geopolymerisation reaction using semi-empirical AM1 calculations. *Cem. Concr. Res.* **2009**, *39*, 1174−1179.
(44) Zhang, Y.; Sun, W.; Li, Z.; Jia, Y. Study of polycondensation process of metakaolin-based geopolymeric cement using semi-empirical AM1 calculations. *Adv. Cem. Res.* **2009**, 67−73.
(45) Yang, C.-S.; Mora-Fonz, J. M.; Catlow, C. R. A. Stability and structures of aluminosilicate clusters. *J. Phys. Chem. C* **2011**, *115*, 24102−24114.
(46) Yang, C.-S.; Mora-Fonz, J. M.; Catlow, C. R. A. Modeling the polymerization of aluminosilicate clusters. *J. Phys. Chem. C* **2012**, *116*, 22121−22128.
(47) White, C. E.; Provis, J. L.; Kearley, G. J.; Riley, D. P.; van Deventer, J. S. J. Density functional modelling of silicate and aluminosilicate dimerisation solution chemistry. *Dalton Trans.* **2011**, *40*, 1348−1355.
(48) White, C. E.; Provis, J. L.; Proffen, T.; van Deventer, J. S. J. Molecular mechanisms responsible for the structural changes occurring during geopolymerization: Multiscale simulation. *AIChE J.* **2012**, *58*, 2241−2253.
(49) Provis, J. L.; Duxson, P.; Lukey, G. C.; Separovic, F.; Kriven, W. M.; van Deventer, J. S. J. Modeling speciation in highly concentrated alkaline silicate solutions. *Ind. Eng. Chem. Res.* **2005**, *44*, 8899−8908.
(50) Feuston, B. P.; Garofalini, S. H. Empirical three-body potential for vitreous silica. *J. Chem. Phys.* **1988**, *89*, 5818.
(51) Garofalini, S. H.; Martin, G. Molecular simulations of the polymerization of silicic acid molecules and network formation. *J. Phys. Chem.* **1994**, *98*, 1311−1316.
(52) Rao, N. Z.; Gelb, L. D. Molecular dynamics simulations of the polymerization of aqueous silicic acid and analysis of the effects of concentration on silica polymorph distributions, growth mechanisms, and reaction kinetics. *J. Phys. Chem. B* **2004**, *108*, 12418−12428.
(53) VandeVondele, J.; Krack, M.; Mohamed, F.; Parrinello, M.; Chassaing, T.; Hutter, J. Quickstep: Fast and accurate density functional calculations using a mixed Gaussian and plane waves approach. *Comput. Phys. Commun.* **2005**, *167*, 103−128.
(54) Lippert, G.; Hutter, J.; Parrinello, M. The Gaussian and augmented-plane-wave density functional method for ab initio molecular dynamics simulations. *Theor. Chem. Acc.* **1999**, *103*, 124−140.
(55) Griebel, M.; Knapek, S.; Zumbusch, G. *Numerical Simulation in Molecular Dynamics: Numerics, Algorithms, Parallelization, Applications*, Vol. 5 of Texts in Computational Science and Engineering; Springer Science & Business Media, 2007.
(56) Manzano, H.; Dolado, J. S.; Griebel, M.; Hamaekers, J. A molecular dynamics study of the aluminosilicate chains structure in Al-rich calcium silicate hydrated (C−S−H) gels. *Phys. Status Solidi A* **2008**, *205*, 1324−1329.
(57) Dolado, J. S.; Griebel, M.; Hamaekers, J. A molecular dynamics study of cementitious calcium silicate hydrate (C−S−H) gels. *J. Am. Chem. Soc.* **2007**, *90*, 3938−3942.
(58) Feuston, B. P.; Garofalini, S. H. Oligomerization in silica sols. *J. Phys. Chem.* **1990**, *94*, 5351−5356.
(59) Stillinger, F. H.; Weber, T. A. Computer simulation of local order in condensed phases of silicon. *Phys. Rev. B* **1985**, *31*, No. 5262.
(60) Griebel, M.; Hamaekers, J. Molecular dynamics simulations of the mechanical properties of polyethylene−carbon nanotube composites. *Handb. Theor. Comput. Nanotechnol.* **2005**, *9*, 409−454.
(61) Engelhardt, G.; Michel, D. *High-Resolution Solid-State NMR of Silicates and Zeolites*; John Wiley & Sons: United States, 1987; p 499.
(62) Lyu, S.-J.; Hsiao, Y.-H.; Wang, T.-T.; Cheng, T.-W.; Ueng, T.-H. Microstructure of geopolymer accounting for associated mechanical characteristics under various stress states. *Cem. Concr. Res.* **2013**, *54*, 199−207.
(63) Fernández-Jiménez, A.; Palomo, A.; Sobrados, I.; Sanz, J. The role played by the reactive alumina content in the alkaline activation of fly ashes. *Microporous Mesoporous Mater.* **2006**, *91*, 111−119.
(64) Malani, A.; Auerbach, S. M.; Monson, P. A. Monte Carlo simulations of silica polymerization and network formation. *J. Phys. Chem. C* **2011**, *115*, 15988−16000.
(65) Humphrey, W.; Dalke, A.; Schulten, K. VMD: visual molecular dynamics. *J. Mol. Graphics* **1996**, *14*, 33−38.
(66) Singh, P. S.; Trigg, M.; Burgar, I.; Bastow, T. Geopolymer formation processes at room temperature studied by $^{29}$Si and $^{27}$Al MAS−NMR. *Mater. Sci. Eng., A* **2005**, *396*, 392−402.
(67) Singh, P. S.; Bastow, T.; Trigg, M. Structural studies of geopolymers by $^{29}$Si and $^{27}$Al MAS−NMR. *J. Mater. Sci.* **2005**, *40*, 3951−3961.
(68) Yamahara, K.; Okazaki, K. Molecular dynamics simulation of the structural development in sol−gel process for silica systems. *Fluid Phase Equilib.* **1998**, *144*, 449−459.
(69) Davidovits, J. Geopolymers: Inorganic polymeric new materials. *J. Therm. Anal.* **1991**, *37*, 1633−1656.
(70) Palomo, Á; Alonso, S.; Fernandez-Jiménez, A.; Sobrados, I.; Sanz, J. Alkaline activation of fly ashes: NMR study of the reaction products. *J. Am. Ceram. Soc.* **2004**, *87*, 1141−1145.
(71) Zhang, Z.; Provis, J. L.; Wang, H.; Bullen, F.; Reid, A. Quantitative kinetic and structural analysis of geopolymers. Part 2. Thermodynamics of sodium silicate activation of metakaolin. *Thermochim. Acta* **2013**, *565*, 163−171.
(72) Mo, B.-h.; Zhu, H.; Cui, X.-m.; He, Y.; Gong, S.-y. Effect of curing temperature on geopolymerization of metakaolin-based geopolymers. *Appl. Clay Sci.* **2014**, *99*, 144−148.
(73) Granizo, N.; Palomo, A.; Fernandez-Jiménez, A. Effect of temperature and alkaline concentration on metakaolin leaching kinetics. *Ceram. Int.* **2014**, *40*, 8975−8985.
(74) Rovnaník, P. Effect of curing temperature on the development of hard structure of metakaolin-based geopolymer. *Constr. Build. Mater.* **2010**, *24*, 1176−1183.
(75) Zhang, M.; Guo, H.; El-Korchi, T.; Zhang, G.; Tao, M. Experimental feasibility study of geopolymer as the next-generation soil stabilizer. *Constr. Build. Mater.* **2013**, *47*, 1468−1478.


DOI: 10.1021/acs.jpcc.8b00697
J. Phys. Chem. C 2018, 122, 6760−6773